Active versus Passive Scalar Turbulence

Antonio Celani,[1] Massimo Cencini,[2] Andrea Mazzino,[3,4] and Massimo Vergassola[2]

[1]*CNRS, INLN, 1361 Route des Lucioles, 06560 Valbonne, France*
[2]*CNRS, Observatoire de la Côte d'Azur, B.P. 4229, 06304 Nice Cedex 4, France*
[3]*ISAC-CNR, Strada Provinciale Lecce-Monteroni Km 1.200, I-73100 Lecce, Italy*
[4]*INFM–Dipartimento di Fisica, Università di Genova, Via Dodecaneso 33, I-16146 Genova, Italy*

(Received 1 July 2002; published 15 November 2002)

Active and passive scalars transported by an incompressible two-dimensional conductive fluid are investigated. It is shown that a passive scalar displays a direct cascade towards the small scales while the active magnetic potential builds up large-scale structures in an inverse cascade process. Correlations between scalar input and particle trajectories are found to be responsible for those dramatic differences as well as for the behavior of dissipative anomalies.

DOI: 10.1103/PhysRevLett.89.234502 PACS numbers: 47.27.–i

The transport of scalar fields by turbulent flows is a common physical phenomenon. The dynamics of the advecting velocity field often depends on the transported field, which is then dubbed *active*. That is, for instance, the case of temperature, affecting the velocity via buoyancy forces. Conversely, situations where the flow is not influenced by the scalar, e.g., for the concentration of a dilute tracer, are referred to as *passive*. Progress has been recently made for the passive case (see Ref. [1] and references therein). These studies put renewed emphasis on the known field-particle duality and long known concepts as intermittency, dissipative anomaly, direct and inverse cascades, usually defined in terms of field characteristics (the Eulerian description), can now be elegantly explained in terms of the statistical properties of particle trajectories (the Lagrangian description). In this Letter, we address the problem of relating the Eulerian properties to the Lagrangian ones for *active* scalar transport.

The active field $a(\boldsymbol{x}, t)$ advected by an incompressible flow $\boldsymbol{v}(\boldsymbol{x}, t)$ is governed by the transport equation

$$\partial_t a + \boldsymbol{v} \cdot \boldsymbol{\nabla} a = \kappa \Delta a + f_a. \tag{1}$$

The passive field $c(\boldsymbol{x}, t)$ evolves *in the same flow* as

$$\partial_t c + \boldsymbol{v} \cdot \boldsymbol{\nabla} c = \kappa \Delta c + f_c. \tag{2}$$

The two scalars have the same diffusion coefficient κ, while f_a and f_c are independent realizations of the same random forcing, with characteristic length scale l_f. The difference between active and passive scalars resides in their relationship with the flow $\boldsymbol{v}$: the active field enters the velocity dynamics, whereas the passive one does not. Here, the evolution equation for $\boldsymbol{v}$ is

$$\partial_t \boldsymbol{v} + \boldsymbol{v} \cdot \boldsymbol{\nabla} \boldsymbol{v} = -\boldsymbol{\nabla} p - \Delta a \boldsymbol{\nabla} a + \nu \Delta \boldsymbol{v}. \tag{3}$$

Equations (1) and (3) are the two-dimensional magnetohydrodynamics equations (see, e.g., Ref. [2]), with the following glossary: a is the scalar magnetic potential; the magnetic field is $\boldsymbol{b} = (-\partial_2 a, \partial_1 a)$; the coupling $-\Delta a \boldsymbol{\nabla} a$ is the Lorentz force $(\boldsymbol{\nabla} \times \boldsymbol{b}) \times \boldsymbol{b}$; the condition $\boldsymbol{\nabla} \cdot \boldsymbol{v} = 0$ is ensured by the pressure term $\boldsymbol{\nabla} p$; and ν is the kinematic viscosity.

Besides its physical relevance (see, e.g., [2]), this example of active scalar is particularly interesting because of the conspicuous differences to its passive counterpart. Namely, while a undergoes an inverse cascade process, i.e., it forms structures at increasingly larger scales [3], c cascades downscale (see Fig. 1). As a consequence, the dissipation of active scalar fluctuations by molecular diffusivity $\epsilon_a = \kappa |\boldsymbol{\nabla} a|^2$ vanishes in the limit $\kappa \to 0$: no dissipative anomaly for the field a. Since the scalar variance is injected at a constant rate F_0 by the source f_a, we have that $e_a(t) = \frac{1}{2} \int a(\boldsymbol{x}, t)^2 d\boldsymbol{x}$ increases linearly in time as $\frac{1}{2} F_0 t$. On the contrary, passive scalar dissipation $\epsilon_c = \kappa |\boldsymbol{\nabla} c|^2$ equals the input $\frac{1}{2} F_0$ and holds c in a statistically stationary state (see Fig. 1).

The probability distribution function (PDF) of a is Gaussian, with zero mean and variance $F_0 t$ (see Fig. 2). This is a straightforward consequence of the vanishing of active scalar dissipation. Indeed, by averaging over the forcing statistics, one obtains: $\partial_t \langle a^{2n} \rangle = n(2n-1) \times F_0 \langle a^{2n-2} \rangle$ (odd moments vanish by symmetry) whose solutions are the Gaussian moments: $\langle a^{2n} \rangle = (2n-1)!! \times (F_0 t)^n$. This may be contrasted with the single-point PDF of c which is stationary and super-Gaussian (see Fig. 2), as generically happens for a passive field sustained by a Gaussian forcing in a rough flow (see, e.g., Ref. [1]).

We now focus on the main purpose of this Letter, which is to investigate the statistical properties of active and passive scalar in the Lagrangian setting. The fundamental property which we exploit is that the equations (1) and (2) can be formally solved in terms of particle propagators. Let $\boldsymbol{X}(s)$ be the trajectory of a fluid particle transported by the flow $\boldsymbol{v}$ and subject to a molecular diffusivity κ, landing at point $\boldsymbol{x}$ at time t. The particle moves according to the stochastic differential equation $d\boldsymbol{X}(s) = \boldsymbol{v}[\boldsymbol{X}(s), s] ds + \sqrt{2\kappa}\, d\boldsymbol{\beta}(s)$, where $\boldsymbol{\beta}(s)$ is a two-dimensional Brownian motion. The probability density

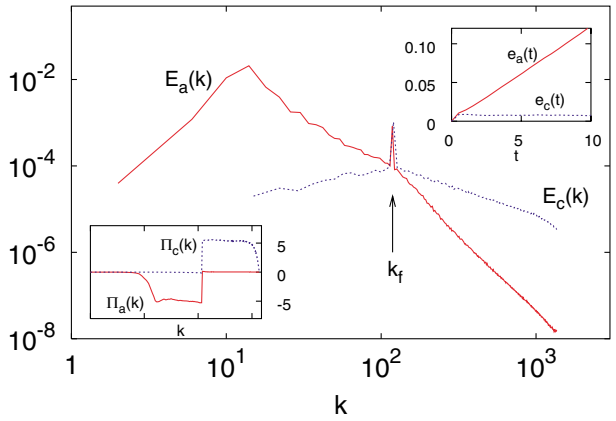

FIG. 1 (color online). Power spectra of active and passive scalar variances $E_a(k) = \pi k|\hat{a}(\boldsymbol{k}, t)|^2$ and $E_c(k) = \pi k|\hat{c}(\boldsymbol{k}, t)|^2$. The fluctuations of a and c injected at the forcing wavelength k_f flow towards smaller and larger wave numbers, respectively. At $k < k_f$ we observe power-law behaviors $E_a(k) \sim k^{-2.0\pm0.1}$ and $E_c(k) \sim k^{0.7\pm0.1}$, while at $k > k_f$ we find $E_a(k) \sim k^{-3.6\pm0.1}$ and $E_c(k) \sim k^{-1.4\pm0.1}$ (for a discussion about the spectra of two- and three-dimensional magnetohydrodynamics, see, e.g., Refs. [3–8]). In the lower left corner, the fluxes of scalar variance $\Pi_{a,c}$ out of wave number k. Negative values indicate an inverse cascade. In the upper right corner, the total scalar variance $e_{a,c}(t) = \int E_{a,c}(k, t)\, dk$. The active variance $e_a(t)$ grows linearly in time, whereas $e_c(t)$ fluctuates around a finite value (see text). The rate of active to passive scalar dissipation is $\epsilon_a/\epsilon_c \simeq 0.005$. The data result from the numerical integration of Eqs. (1)–(3) by a dealiased pseudo-spectral parallel code, on a doubly periodic box of size 2π and resolution 4096^2. The forcing terms f_a and f_c are homogeneous independent Gaussian processes with zero mean and correlation $\langle \hat{f}_i(\boldsymbol{k}, t)\hat{f}_j(\boldsymbol{k}', t')\rangle = [F_0/(2\pi k_f)]\delta_{ij}\delta(\boldsymbol{k} + \boldsymbol{k}')\delta(k - k_f)\delta(t - t')$ where $i, j = a, c$. The coefficients κ and ν are chosen to obtain a dissipative length scale of the order of the smallest resolved scales. All fields are set to zero at $t = 0$, and time is defined in units of eddy-turnover time $\tau = l_f/v_{\text{rms}}$ where $l_f = 2\pi/k_f$.

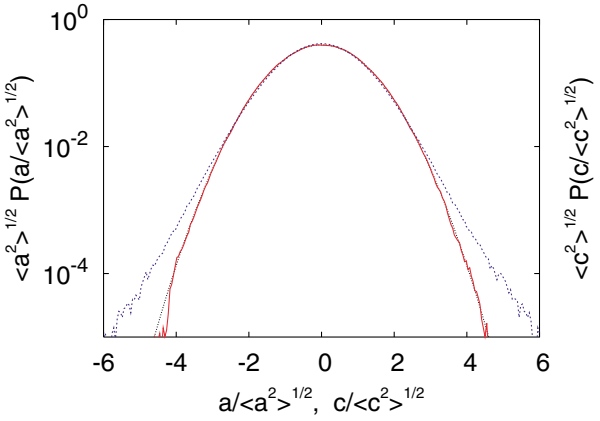

FIG. 2 (color online). PDF's of active (solid line) and passive (dashed line) scalar fields normalized by their standard deviation. The active scalar PDF is indistinguishable from a Gaussian (dotted line).

$p(\boldsymbol{y}, s \mid \boldsymbol{x}, t)$ of finding a particle at point $\boldsymbol{y}$ and time $s \le t$ obeys the Kolmogorov equations (see, e.g., [9]):

$$-\partial_s p(\boldsymbol{y}, s \mid \boldsymbol{x}, t) - \boldsymbol{\nabla}_y \cdot [\boldsymbol{v}(\boldsymbol{y}, s)p(\boldsymbol{y}, s \mid \boldsymbol{x}, t)] = \kappa\Delta_y p(\boldsymbol{y}, s \mid \boldsymbol{x}, t), \quad (4)$$

$$\partial_t p(\boldsymbol{y}, s \mid \boldsymbol{x}, t) + \boldsymbol{\nabla}_x \cdot [\boldsymbol{v}(\boldsymbol{x}, t)p(\boldsymbol{y}, s \mid \boldsymbol{x}, t)] = \kappa\Delta_x p(\boldsymbol{y}, s \mid \boldsymbol{x}, t). \quad (5)$$

The unusual minus signs in the left-hand side of (4) are due to the fact that particles move *backward* in time. The solution of (1) and (2) can be written in terms of the propagator:

$$a(\boldsymbol{x}, t) = \int_0^t ds \int d\boldsymbol{y}\, f_a(\boldsymbol{y}, s)p(\boldsymbol{y}, s \mid \boldsymbol{x}, t), \quad (6)$$

$$c(\boldsymbol{x}, t) = \int_0^t ds \int d\boldsymbol{y}\, f_c(\boldsymbol{y}, s)p(\boldsymbol{y}, s \mid \boldsymbol{x}, t), \quad (7)$$

as can be directly checked by inserting (6) and (7) in (1) and (2), respectively, and utilizing (5). It is important to notice that both the active and the passive scalar are expressed in terms of *the same propagator* p, since a and c are advected by the same velocity field. Equation (6) can be written more compactly as $a(\boldsymbol{x}, t) = \langle \int_0^t f_a(\boldsymbol{X}(s), s)ds\rangle_X$, where $\langle\cdots\rangle_X$ denotes the average over particle trajectories, and similarly for Eq. (7).

The interpretation of Eqs. (6) and (7) is that the value of the scalar field at $(\boldsymbol{x}, t)$ is given by the superposition of the input along all trajectories eventually convening at that point and time. It is worth remarking that, even in the limit of vanishing diffusivity, the particle propagator does not collapse onto a single trajectory, as expected for incompressible rough flows [1]. The differences between active and passive fields are due to the correlations between the propagator p and the forcing f_a, which are absent, by definition of passive transport, between p and f_c. Indeed, via the coupling term in Eq. (3), f_a affects the velocity field and, consequently, the evolution of the propagator p. To further clarify the relationship between Lagrangian trajectories and active field forcing, it is necessary to investigate the evolution of the particle propagator. The problem is that p evolves *backward* in time, according to (4), and the condition $p(\boldsymbol{y}, t \mid \boldsymbol{x}, t) = \delta(\boldsymbol{y} - \boldsymbol{x})$ is set at the final time t. Contrary to a usual forward integration, where $\boldsymbol{v}$ and p can be advanced in parallel, a brute force backward integration would require the storage of velocity configurations for the whole lapse of integration which is quite unfeasible. To overcome this problem, we devised a fast and low-memory demanding algorithm to integrate numerically Eqs. (1), (3), and (4) [10].

Let us sketch the basic idea of the algorithm. We proceed inductively and first consider the case $t = t_1 = \Delta t$, i.e., a single step. The fields $a(0)$ and $\boldsymbol{v}(0)$ and the final condition $p(t_1)$ are given as input (we omit spatial dependences). The fields $a(t_1)$ and $\boldsymbol{v}(t_1)$ are obtained by a forward integration whose numerical cost is denoted c_f.

The propagator is then evolved backward, at a cost denoted c_b, to obtain $p(0)$. The total cost of the procedure is $C_1 = c_f + c_b$. Consider now the case $t = t_N = (2^N - 1)\Delta t$. Our aim is to show that the algorithm for $2^N - 1$ steps can be split into two successive applications with $2^{N-1} - 1$ steps and thus lends to a recursive procedure. Integrating forward $a(0)$, $\boldsymbol{v}(0)$ for 2^{N-1} steps give $a(t_{N-1} + \Delta t)$ and $\boldsymbol{v}(t_{N-1} + \Delta t)$ at a cost $2^{N-1}c_f$. Those fields, together with $p(t_N)$, are the input for the algorithm in the interval $[t_{N-1} + \Delta t, t_N]$, which gives $p(t_{N-1} + \Delta t)$ at a cost C_{N-1}. A backward step is finally needed to obtain $p(t_{N-1})$. With this field and $a(0)$, $\boldsymbol{v}(0)$ we can now apply the algorithm in the first half of the interval $[0, t_{N-1}]$ to get $p(0)$. The computational cost is $c_b + C_{N-1}$. Summing up all the costs we have the recursive relation $C_N = 2^{N-1}c_f + 2C_{N-1} + c_b$, with solution $C_N = \frac{N}{2}2^N c_f + (2^N - 1)c_b$. Comparing C_N with the cost of a forward integration of Eqs. (1), (3), and (5), that is, $(c_f + c_b)(2^N - 1)$, we have an increase by a factor $\approx \{c_f/[2(c_f + c_b)]\}N$, i.e., logarithmic in the number of time steps. As for memory requirements, only the N couples of fields $a(t_N - t_k)$, $\boldsymbol{v}(t_N - t_k)$, $k = 1, \ldots, N$ need to be stored—again a logarithmic factor.

A typical evolution of the propagator is shown in the central column of Fig. 3. We can now reconstruct the time sequence of the forcing contributions $\phi_{a,c}(s) = \int d\boldsymbol{y}\, f_{a,c}(\boldsymbol{y}, s)p(\boldsymbol{y}, s \mid \boldsymbol{x}, t)$ which, integrated over s, gives the amplitude of the scalar fields according to (6) and (7). As shown in Fig. 4, the time series of $\phi_a(s)$ and $\phi_c(s)$ are markedly different. In the active scalar case, the sequence is strongly skewed towards positive values at all times. This signals that the trajectories preferentially select regions where f_a has a positive sign, summing up forcing contributions to generate a typical variance of a of the order $F_0 t$. Conversely, f_c can be positive or negative with equal probability on distant trajectories, and the time integral in Eq. (7) averages out to zero for $|s - t| > \tau$ ($\tau = l_f/v_{\mathrm{rms}}$ is the eddy-turnover time). Therefore, typically $c^2 \sim F_0\tau$. The cumulative effect of the correlation between forcing and propagator is even more evident from the relation $\int_0^s \phi_a(s')\, ds' = \int d\boldsymbol{y}\, a(\boldsymbol{y}, s)p(\boldsymbol{y}, s \mid \boldsymbol{x}, t)$ derived from (1) and (4). As shown in Fig. 4, the growth of the scalar variance is thus related to a strong spatial correlation between the propagator and the active field. That is further evidenced by comparing the first and the second columns of Fig. 3: the distribution of particles closely follows the distribution of like-sign active scalar. This amounts to saying that large-scale scalar structures are built out of smaller ones which "coalesce" together [3]. This situation has to be contrasted with the absence of large-scale correlations between the propagator and the passive scalar field (second and third columns of Fig. 3).

As remarked previously, the absence of dissipative anomaly is closely related to the onset of an inverse cascade. Let us now discuss this issue from a Lagrangian viewpoint and consider the squared active field a^2. On one hand, it can be written as the square of (6). On the other hand, one can multiply (1) by $2a$ to obtain the equation $\partial_t a^2 + \boldsymbol{v} \cdot \nabla a^2 = \kappa \Delta a^2 + 2af_a - 2\epsilon_a$ and solve it for $\epsilon_a = 0$ in terms of particle trajectories. The comparison of the two previous expressions yields

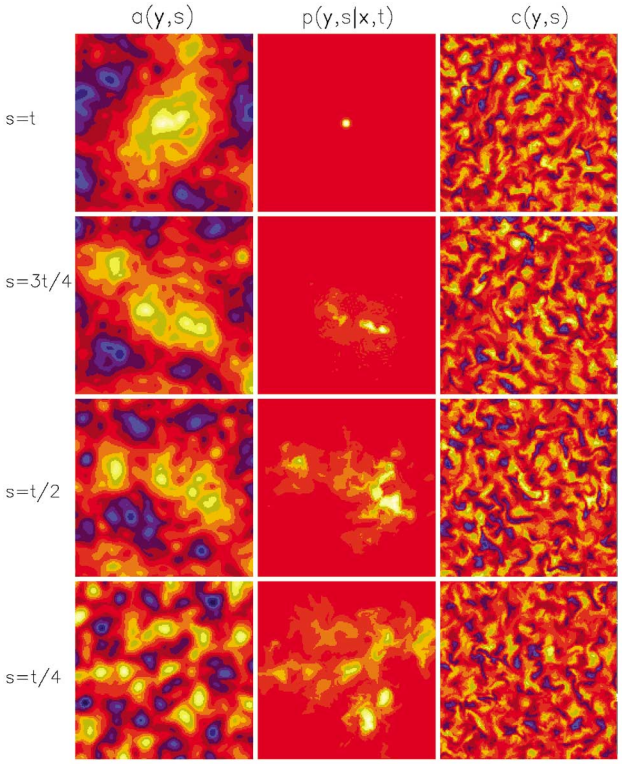

FIG. 3 (color online). Time runs from bottom to top. First column: time evolution of the active scalar field resulting from the numerical integration of Eqs. (1) and (3). Second column: backward evolution of the particle propagator according to Eq. (4). Third column: time evolution of the passive scalar field in the same flow.

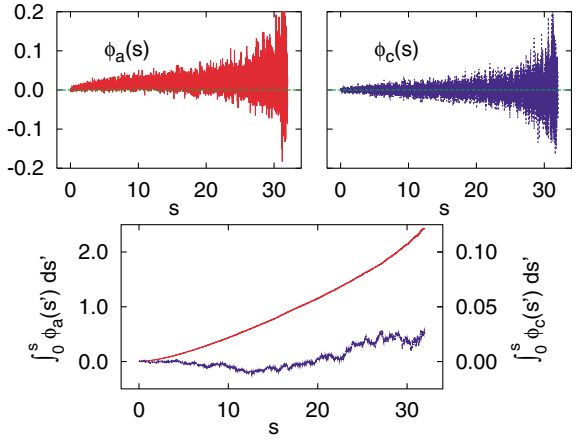

FIG. 4 (color online). Top: $\phi_{a,c}(s) = \int d\boldsymbol{y}\, f_{a,c}(\boldsymbol{y}, s)p(\boldsymbol{y}, s \mid \boldsymbol{x}, t)$. The two graphs have the same scale on the vertical axis. Here, $t = 32$. Bottom: time integrals $\int_0^s \phi_a(s')\, ds'$ (upper curve) and $\int_0^s \phi_c(s')\, ds'$ (lower curve). Note the different scale on the vertical axis. Recall that $\int_0^t \phi_a(s')\, ds' = a(\boldsymbol{x}, t)$ (and similarly for c).

$$\int_0^t ds \int_0^t ds' \iint f_a(\mathbf{y}, s) f_a(\mathbf{y}', s') p(\mathbf{y}, s \mid \mathbf{x}, t) p(\mathbf{y}', s' \mid \mathbf{x}, t) = \int_0^t ds \int_0^t ds' \iint f_a(\mathbf{y}, s) f_a(\mathbf{y}', s') p(\mathbf{y}', s'; \mathbf{y}, s \mid \mathbf{x}, t), \quad (8)$$

where $p(\mathbf{y}', s'; \mathbf{y}, s \mid \mathbf{x}, t) = p(\mathbf{y}, s \mid \mathbf{x}, t) p(\mathbf{y}', s' \mid \mathbf{y}, s)$ denotes the probability that a trajectory ending in $(\mathbf{x}, t)$ was in $(\mathbf{y}, s)$ and $(\mathbf{y}', s')$. Integration over $\mathbf{y}$ and $\mathbf{y}'$ is implied. To obtain the right-hand side of (8), consider the expression $a^2(\mathbf{x}, t) = 2 \int_0^t ds \int d\mathbf{y} f_a(\mathbf{y}, s) a(\mathbf{y}, s)$, insert $a(\mathbf{y}, s) = \int_0^s ds' \int d\mathbf{y}' f_a(\mathbf{y}', s')$, i.e., Eq. (6) evaluated at time s, and exploit the symmetry under exchange of s and s' to switch from a time-ordered form to a time-symmetric one to get rid of the factor 2.

Notice as a side remark that by integrating the right-hand side of (8) over $\mathbf{x}$, exploiting the normalization $\int d\mathbf{x} p(\mathbf{y}, s \mid \mathbf{x}, t) = 1$ [as follows from (5)], and averaging over the forcing statistics, one obtains $\langle a^2 \rangle = F(0)t$. The result can be generalized to show that $\langle a^{2n} \rangle = (2n-1)!![F(0)t]^n$, in agreement with the Eulerian argument for the Gaussianity of the single-point PDF of a given above.

Equation (8) can be recast as $\langle \int_0^t f_a(\mathbf{X}(s), s) ds \rangle_X^2 = \langle [\int_0^t f_a(\mathbf{X}(s), s) ds]^2 \rangle_X$, leading to the conclusion that $\int_0^t f_a(\mathbf{X}(s), s) ds$ is a *nonrandom* variable over the ensemble of trajectories. This result has a simple interpretation: the absence of dissipative anomaly (i.e., $\epsilon_a = 0$) is equivalent to the property that along any of the infinite trajectories $\mathbf{X}(s)$ ending in $(\mathbf{x}, t)$ the quantity $\int_0^t f_a(\mathbf{X}(s), s) ds$ is exactly the same and equals $a(\mathbf{x}, t)$. Therefore, a single trajectory suffices to obtain the value of $a(\mathbf{x}, t)$ contrary to the passive case, where different trajectories contribute disparate values of $\int_0^t f_c(\mathbf{X}(s), s) ds$, with a typical spread $\epsilon_c t$. In this case, only the average over all trajectories yields the correct value of $c(\mathbf{x}, t)$.

The previous property extends to multiple points. Proceeding as for (8), one can show that m trajectories are enough to calculate the product of arbitrary powers of a at m different points. In particular, structure functions $\langle (a(\mathbf{r}) - a(\mathbf{0}))^n \rangle$ for any order n can be shown to involve only two trajectories. This should be contrasted with the passive scalar, where the number of trajectories increases with n, and this is at the core of anomalous scaling of the field [1]. Indeed, we do not observe any anomalous scaling for the structure functions of the active field a and the PDF's of its increments are self-similar. Note that the same phenomenon and a lack of dissipative anomaly were also found for a passive scalar in a compressible flow [11]. In that case, the ensemble of trajectories collapses onto a unique path, fulfilling in the simplest way the constraint (8) and its multipoint analogs. Here, even though the trajectories do not collapse, the constraints are satisfied due to the subtle correlation between forcing and trajectories peculiar to the active case.

We conclude with the following open issue. It is known that passive correlation functions are controlled by the asymptotically dominant terms in particle propagators (see, e.g., Ref. [1]). Is this also true for active scalars? The correlations between propagator and input in (6) suggest this is not the general rule. For some specific systems, those correlations might, however, be such that the asymptotics of the propagator still stands out at large times [12,13]. Clarifying the dynamical conditions controlling this phenomenon will be the subject of future work.

We are grateful to A. Noullez and I. Procaccia for useful discussions. This work has been supported by the EU under Contract No. HPRN-CT-2000-00162, and by Indo-French Center for Promotion of Advanced Research (IFCPAR 2404-2). A. M. has been partially supported by Cofin2001 (prot.2001023842). Numerical simulations have been performed at IDRIS (Project No. 021226) and at CINECA (INFM parallel computing initiative).

[1] G. Falkovich, K. Gawędzki, and M. Vergassola, Rev. Mod. Phys. **73**, 913 (2001).
[2] D. Biskamp, *Nonlinear Magnetohydrodynamics* (Cambridge University, Cambridge, U.K., 1993).
[3] D. Biskamp and U. Bremer, Phys. Rev. Lett. **72**, 3819 (1994).
[4] A. Pouquet, J. Fluid Mech. **88**, 1 (1978).
[5] S. Sridhar and P. Goldreich, Astrophys. J. **432**, 612 (1994).
[6] M. K. Verma, D. A. Roberts, M. L. Goldstein, S. Ghosh, and W. T. Stribling, J. Geophys. Res. **101**, 21619 (1996).
[7] H. Politano, A. Pouquet, and V. Carbone, Europhys. Lett. **43**, 516 (1998).
[8] D. Biskamp and E. Schwarz, Phys. Plasmas **8**, 3282 (2001).
[9] H. Risken, *The Fokker Planck Equation* (Springer-Verlag, Berlin, 1998).
[10] We thank A. Noullez for illuminating suggestions on the algorithm.
[11] K. Gawędzki and M. Vergassola, Physica (Amsterdam) **138D**, 63 (2000).
[12] E. S. C. Ching, Y. Cohen, T. Gilbert, and I. Procaccia, nlin.CD/0111030 [Europhys. Lett. (to be published)]; nlin.CD/0207005.
[13] A. Celani, T. Matsumoto, A. Mazzino, and M. Vergassola, Phys. Rev. Lett. **88**, 054503 (2002).